Eur. Phys. J. D (2020) 74: 223
https://doi.org/10.1140/epjd/e2020-10409-8

THE EUROPEAN PHYSICAL JOURNAL D

Regular Article

# Structural evolution in boron-based clusters $B_5Al_n^{0/-/+}(n = 1-4)$: Al atoms transition from the periphery of the planar W-shaped $B_5$ ring to the vertex of the bipyramid*

Limei Wen[1,2], Guoliang Li[1,a], Li-Ming Yang[2,b], and Eric Ganz[3]

[1] Key Laboratory of Theoretical Chemistry of Environment, Ministry of Education; Center for Computational Quantum Chemistry, School of Chemistry, South China Normal University, Guangzhou 510006, P.R. China
[2] Hubei Key Laboratory of Bioinorganic Chemistry and Materia Medica, Key Laboratory of Material Chemistry for Energy Conversion and Storage, Ministry of Education, Hubei Key Laboratory of Materials Chemistry and Service Failure, School of Chemistry and Chemical Engineering, Huazhong University of Science and Technology, Wuhan 430074, P.R. China
[3] School of Physics and Astronomy, University of Minnesota, 115 Union St. SE, Minneapolis, Minnesota 55455, USA

Received 23 July 2020 / Received in final form 7 September 2020 / Accepted 10 September 2020
Published online 1 November 2020


**Abstract.** The structures and properties of binary boron-aluminum $B_5Al_n^{0/-/+}(n = 1-4)$ clusters have been systematically explored using the density functional theory method at the B3LYP/6–311+G(d) level and the coupled cluster method at the CCSD(T)/6–311+G(2df)//B3LYP/6–311+G(d) level. Lowest-energy structures, stabilities, growth behaviors and chemical bonding of these clusters were analyzed. Our results show that when the number of doped Al atoms is one or two, the Al atoms are located at the periphery, and the host $B_5$ cluster preferentially forms a W-shape core, which is only slightly affected by the Al atoms. When there are three or four Al atoms, the $B_5Al_n^{0/-/+}(n = 3, 4)$ clusters have their lowest energy structures preferentially in capped bipyramid configurations. Neutral $B_5Al_n(n = 1, 3)$ clusters are somewhat more stable than their neighboring n clusters, while anionic and cationic $B_5Al_n^{-/+}(n = 2, 4)$ clusters tend to be somewhat more stable. We also simulated the infrared (IR) spectrum and photoelectron spectroscopy (PES) of these clusters for future experimental comparison. Adaptive natural density partitioning (AdNDP) analysis shows that a variety of delocalized multicenter bonds appear in these clusters, which may enhance the stability of the clusters.

## 1 Introduction

Recent experimental studies showed that metal nanocomposites have been prepared based on $\gamma$-cyclodextrins ($\gamma$-CDs) and boron clusters, and boron clusters play an important role of reductant and stabilizer in this process [1]. Coincidentally, experimental and theoretical studies on boron clusters-based persistent phosphors reported that the phosphors exhibit excellent luminescence properties, and revealed that non-metallic/heavy-atom boron clusters may be used to prepare high-performance phosphors [2]. Systematic studies of pure boron clusters by Wang and coworkers showed that pure boron clusters have relatively large-sized planar or quasi-planar (2D) structures [3–6]. There have been important advancements both experimentally and theoretically in the study of the electronic stability, bonding properties, and chemical reactivity of the famous closo-$[B_nX_n]^{2-}$ dianions as function of the boron cage scaffold number $n$ ($n$ = 12, 11, 10, 6) as well as the ligand $X$ ($X$ = H, F, Cl, Br, I, At, CN) in recent years [7–11].

Structures and properties of binary clusters show tunability and flexibility compared with those of pure clusters. Researchers studied the metal-doped boron clusters, such as the structural growth pattern of $B_nNi_m$ ($n$ = 2–22, $m$ = 1–2) clusters using density functional theory calculations, with the results showing that $B_{14}Ni$ and $B_{22}Ni_2$ were outstanding species with surprising geometric structure, enhanced thermodynamic stability and large average binding energy [12]. Theoretical studies on the hydrogen adsorption capacity of magnesium-doped boron clusters ($Mg_2B_n$, $n$ = 4–14) found that the $Mg_2B_6$ cluster has the largest $H_2$ adsorption capacity at ambient temperature

* Supplementary material in the form of one pdf file available from the Journal web page at https://doi.org/10.1140/epjd/e2020-10409-8.

[a] e-mail: glli@scnu.edu.cn
[b] e-mail: Lmyang@hust.edu.cn

and pressure [13]. And studies of beryllium-doped boron clusters $BeB_n^{0/-}$ ($n$ = 10–20) revealed that a novel and fascinating planar $BeB_{16}^-$ cluster with $C_{2v}$ symmetry has robust relative stability [14].

Boron and aluminum are both group 13 elements and have the same valence shell ($ns^2np^1$). Thus, they can easily form mixed binary clusters with different ratios. Recent experimental progress has shown that boron-aluminum binary clusters are unique in structures and properties. Wang and coworkers systematically studied aluminum-doped boron clusters using both photoelectron spectroscopy and high-level ab initio calculations [15–17]. These studies revealed a series of interesting phenomena. $B_7^-$ and $B_{12}^-$ clusters each had one Al atom substituted for a B atom to form planar $AlB_6^-$ and $AlB_{11}^-$ structures [15]. For $AlB_9^-$ and $AlB_{10}^-$, the Al atoms were observed in the periphery, avoiding the central position [16]. In the case of the molecular wheels $B_8^-$ and $B_9^-$, umbrella structures $AlB_7^-$ and $AlB_8^-$ were formed [17]. Furthermore, a recently published paper shows that $AlB_6$ nanosheets have very high stability, unexpected structure motifs, triple Dirac cones, node-loop features and surprisingly high predicted superconducting critical temperature under strain [18].

These results have stimulated our interest in studies of boron-aluminum clusters. In last study, we have conduct a systematic investigation on boron-aluminum clusters $B_4Al_n^{0/-/+}(n = 1–5)$ using density functional theory (DFT) method and high-level coupled cluster single-double and perturbative triple [CCSD(T)] method with the results showing that Al atoms tend to occupy the periphery sites of the clusters and the structures change from 2D to 3D configuration as $n$ increases [19]. To further explore the structures and properties of boron-aluminum clusters, a detailed study of the $B_5Al_n^{0/-/+}(n = 1–4)$ clusters was presented in this article, using similar theoretical method as before. Generally, the geometric structures, stabilities, electronic properties, and chemical bonding properties of $B_5Al_n^{0/-/+}$ ($n$=1–4) clusters were explored using DFT and CCSD(T) methods. First, the energies and structural stabilities of various $B_5Al_n^{0/-/+}$ ($n$=1–4) isomers were calculated. Second, the electronic properties of the most stable $B_5Al_n^{0/-/+}$ isomers were explored using their binding energies ($E_b$), fragmentation energies ($\Delta_1$E), second-order differences of the total energies ($\Delta_2E$), HOMO–LUMO gaps (For open shell species, the calculated HOMO–LUMO gaps refer to the SOMO–LUMO gaps), ionization potentials (IP), and electron affinities (EA). Third, the simulated infrared (IR) spectra and photoelectron spectroscopy (PES) of the isomers were calculated. Finally, the bond structures of the isomers were investigated using AdNDP analysis.

## 2 Computational methods

Similar computational methods have been employed as those for the $B_4Al_n^{0/-/+}$ ($n$=1–5) system before [19]. Thus the global minimum structures of the $B_5Al_n^{0/-/+}$ ($n$=1–4) clusters were searched using the Coalescence Kick (CK) program [20]. All the CK optimizations were performed with the DFT-B3LYP hybrid functional [21, 22] and the 3-21G basis set [23]. Then, the structures were re-optimized using same B3LYP method but larger 6−311+G(d) basis set [24]. Selecting the low-lying structures and using their symmetries, harmonic vibration frequency analyses were performed at the same B3LYP/6−311+G(d) level. During the structural search, the two lowest-energy spin states, i.e. the singlet and triplet for even number electrons systems, and the doublet and quadruplet for odd number electrons systems, were considered for each $B_5Al_n^{0/-/+}$ cluster. Finally, high-level CCSD(T) method [25] and larger 6−311+G(2df) basis set were used to calculate reliable final energies for structures with relative energies less than 20 kcal/mol. Structural optimizations with the B3LYP/6–311+G(d) method followed by high-level CCSD(T)/6–311+G(2df) single point computations to refine the energies have also been successfully used for boron–aluminum clusters in previous work [15–17].

To guide future experimental work, we simulated the vertical detachment energies (VDEs) for the lowest energy isomers of anionic $B_5Al_n^-$ ($n$=1–4) clusters using the time-dependent DFT (TDDFT) method at the TD-B3LYP/6–311+G(d) level. The first VDE value of each cluster was calculated as the energy difference between the lowest energy structure of the anionic cluster and the corresponding neutral one. Other excited state energies were added to the first VDE value to obtain the higher VDEs. For the lowest energy structures with open shells, such as those of the $B_5Al^-$ and $B_5Al_3^-$ clusters, the first two VDE values were calculated as the energy differences between the doublet ground states of the anions and the final lowest-lying singlet and triplet of the neutral clusters with anionic geometry, respectively. The higher VDE values were calculated by adding the corresponding vertical excitation energies for the singlet and triplet states of the neutral species to the two lowest VDEs. We also performed adaptive natural density partitioning (AdNDP) [26–29] analysis to interpret the chemical bonding of the lowest energy $B_5Al_n^{0/-/+}$ ($n$=1–4) clusters. All of the DFT and CCSD(T) calculations were carried out with the Gaussian 09 program [30], and all of the AdNDP analyses were performed using the Multiwfn 3.6 software [31].

## 3 Results and discussion

### 3.1 Structural evolution of the Al-doped boron clusters

Figures 1–3 show numerous low-energy structures of the $B_5Al_n^{0/-/+}$ ($n$=1–4) clusters. These are ranked according to the reliable CCSD(T)/6–311+G(2df)//B3LYP/6–311+G(d) energies. In the following discussion, we will mainly consider these CCSD(T) energies for the structure energies, while the HOMO–LUMO gap is at the B3LYP level. We also found some other $B_5Al_n^{0/-/+}$ ($n$=1–4) structures with their relative energies within ~20 kcal/mol, which are included in Figures S1–S3.

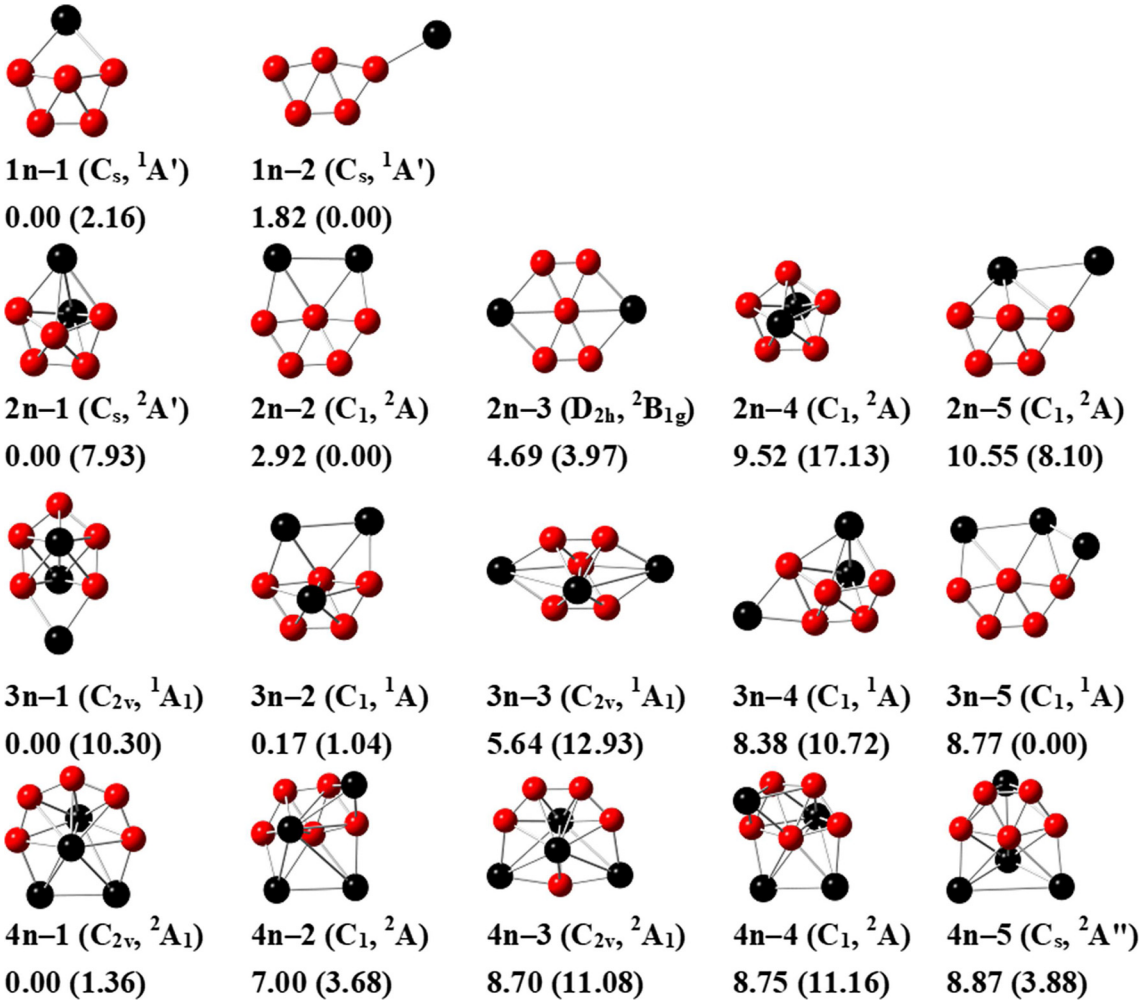


**Fig. 1.** Optimized geometries for neutral $B_5Al_n$ ($n=1$–4) clusters. The relative energies (in kcal/mol, under each structure) were obtained at the CCSD(T)/6–311+G(2df)//B3LYP/6–311+G(d) and B3LYP/6–311+G(d) (in parentheses) levels of theory.

#### 3.1.1 Neutral $B_5Al_n$ ($n=1$–4) clusters

For the $B_5Al$ cluster, the lowest energy configuration $1n-1$ has five boron atoms forming a W-like structure, and a single Al atom in a bridge configuration (see Fig. 1). The next configuration has 1.82 kcal/mol higher energy. Both structures $1n-1$ and $1n-2$ can be obtained by adding an Al atom directly to the lowest energy configuration of a pure $B_5$ cluster [32]. Structures $1n-1$ and $1n-2$ are consistent with the first two $B_5Al$ structures reported by Feng et al. [33] and by Böyükata et al. [34].

For the $B_5Al_2$ cluster, the lowest energy isomer $2n$–1 has a 3D structure, and this can be created by capping an Al atom onto the surface of the $B_5Al$ structure $1n$–1. Structure $2n$–2 lies 2.92 kcal/mol above $2n$–1, and this can be created by adding two Al atoms to the lowest energy structure of the pure $B_5$ cluster. The HOMO–LUMO energy gap of isomer $2n$–1 is 2.48 eV, which is larger than the 1.86 eV gap of isomer $2n$–2, indicating that isomer $2n$–1 is chemically more stable.

For the $B_5Al_3$ cluster, the lowest energy structure $3n-1$ has a 3D hexagonal bipyramid configuration with $C_{2v}$ symmetry and $^1A_1$ electronic state. Isomer $3n$–2, having slightly higher energy (0.17 kcal/mol) than $3n$–1, can be obtained by capping an Al atom onto the surface of the $B_5Al_2$ structure $2n$–2. The HOMO–LUMO gap of isomer $3n$–1 is 1.71 eV, which is smaller than the 2.59 eV gap of isomer $3n$–2, and the difference in energy is only 0.17 kcal/mol indicating that isomer $3n$–2 may compete with $3n$–1 to become the global minimum of the $B_5Al_3$ cluster. Other higher energy isomers $3n$–3, $3n$–4 and $3n$–5 can be obtained by adding an Al atom to the periphery of the $B_5Al_2$ structures $2n$–3, $2n$–1 and $2n$–2, respectively.

For the $B_5Al_4$ cluster, the lowest energy structure $4n-1$ has 3D heptagonal bipyramid configuration with $C_{2v}$ symmetry and $^2A_1$ electronic state. The relative energy of other low-energy $B_5Al_4$ isomers are higher than $4n$–1 by more than 7.00 kcal/mol, so we can predict that structure $4n$–1 is the global minimum of the $B_5Al_4$ cluster.

#### 3.1.2 Anionic $B_5Al_n^-$ (n = 1–4) clusters

The low-energy isomers for anionic $B_5Al_n^-$ ($n=1$–4) clusters are listed in Figure 2. Some higher-energy isomers

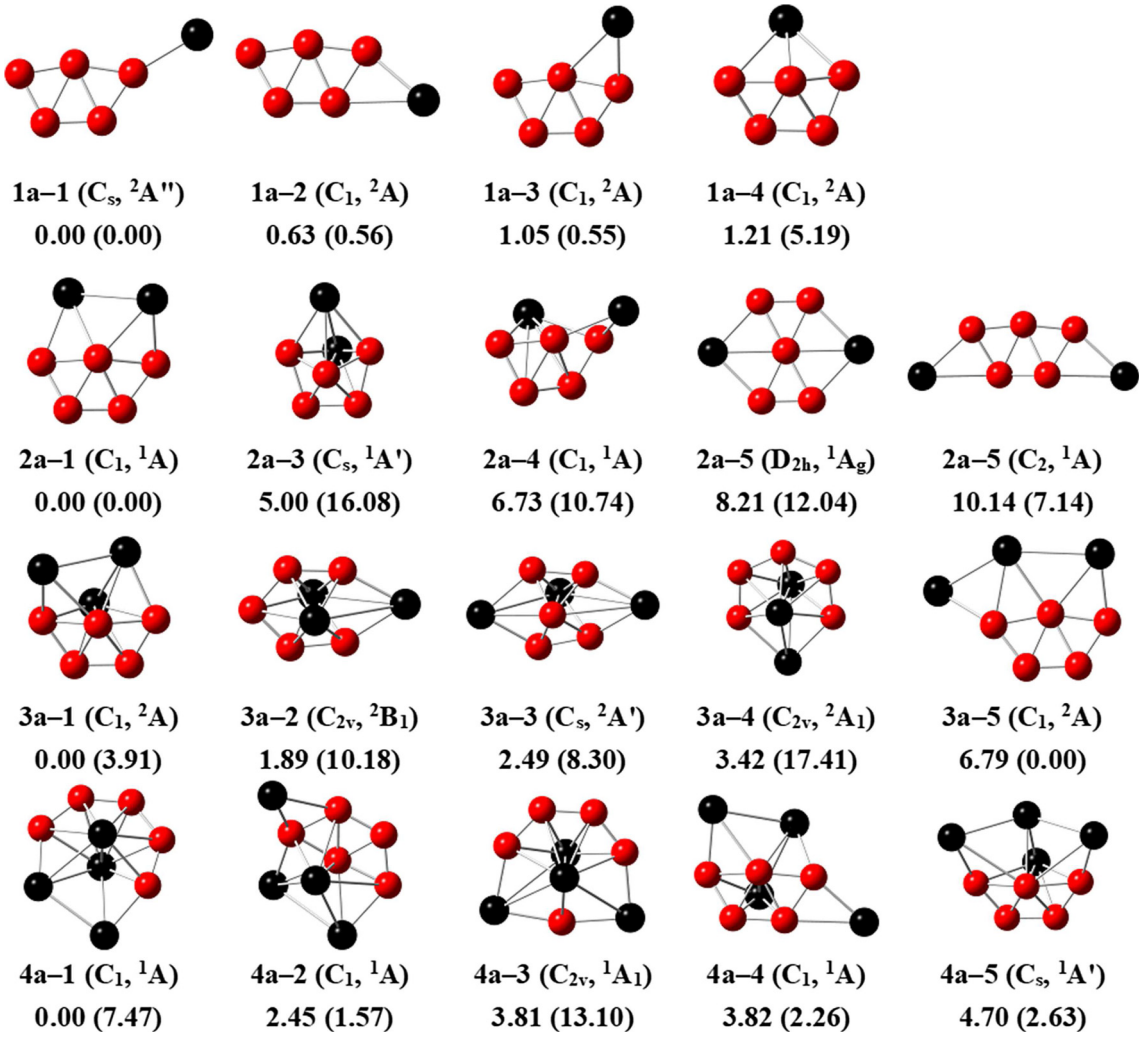


**Fig. 2.** Optimized geometries for anionic $B_5Al_n^-$ ($n=1$–4) clusters. The relative energies (in kcal/mol, under each structure) were obtained at the CCSD(T)/6–311+G(2df)//B3LYP/6–311+G(d) and B3LYP/6–311+G(d) (in parentheses) levels of theory.

are listed in Figure S2. For the $B_5Al^-$ cluster, the lowest energy structure 1*a*–1 with planar 2D configuration and $C_s$ symmetry is similar to structure 1*n*–2 of the neutral $B_5Al$ cluster. Comparing structure 1*a*–1 with structure 1*n*–2, we find that the B–B bond length hardly changed, but the B–Al bond changed from 2.207 Å to 2.079 Å. Thus, the B–Al bond is shorter and stronger in 1*a*–1. Isomers 1*a*–2, 1*a*–3 and 1*a*–4 are only 0.63, 1.05 and 1.21 kcal/mol higher in energy than structure 1*a*–1, respectively. The HOMO–LUMO gaps of isomers 1*a*–2, 1*a*–3 and 1*a*–4 are 1.84, 1.84 and 2.36 eV, respectively. These are all higher than the 1.76 eV gap of 1*a*–1, indicating that they all may be favorable structures for the anionic $B_5Al^-$ cluster.

For the $B_5Al_2^-$ cluster, the lowest energy structure 2*a*–1 with quasi-planar configuration is similar to structure 2*n*–2 of the neutral $B_5Al_2$ cluster. Comparing structure 2*a*–1 with structure 2*n*–2, we find that adding an electron leaves the B–B bond lengths relatively unchanged, but the B–Al and Al–Al bond lengths become longer. Isomer 2*a*–2 with $C_s$ symmetry and $^1A'$ electronic state has 5.00 kcal/mol higher energy than structure 2*a*–1, so we can deduce that structure 2*a*–1 will be preferred experimentally. There are other higher energy isomers of anionic $B_5Al_2^-$ cluster, for example, isomer 2*a*–3, which can be formed by adding an Al atom to structure 1*a*–4. Since we will see below that the lowest energy structures of anionic $B_5Al_n^-$ ($n=3$, 4) clusters have 3D configuration, $n=2$ can be regarded as the transition point from 2D to 3D structures.

For the $B_5Al_3^-$ cluster, the lowest energy structure 3*a*–1 with 3D configuration can be obtained by capping an Al atom on the surface of structure 2*a*–1. This is geometrically similar to structure 3*n*–2. Isomer 3*a*–2 with higher energy (by 1.89 kcal/mol) can be formed by adding an electron to structure 3*n*–1. The HOMO–LUMO gap of isomer 3*a*–1 is 2.07 eV, which is slightly larger than the 1.98 eV gap of isomer 3*a*–2. Other $B_5Al_3^-$ isomers have even higher energies, so structure 3*a*–1 should be the dominant structure of the anionic $B_5Al_3^-$ cluster.

For the $B_5Al_4^-$ cluster, the lowest energy structure 4*a*–1 with heptagonal bipyramidal structure is similar to structure 4*n*–1 of the neutral $B_5Al_4$ cluster. Other

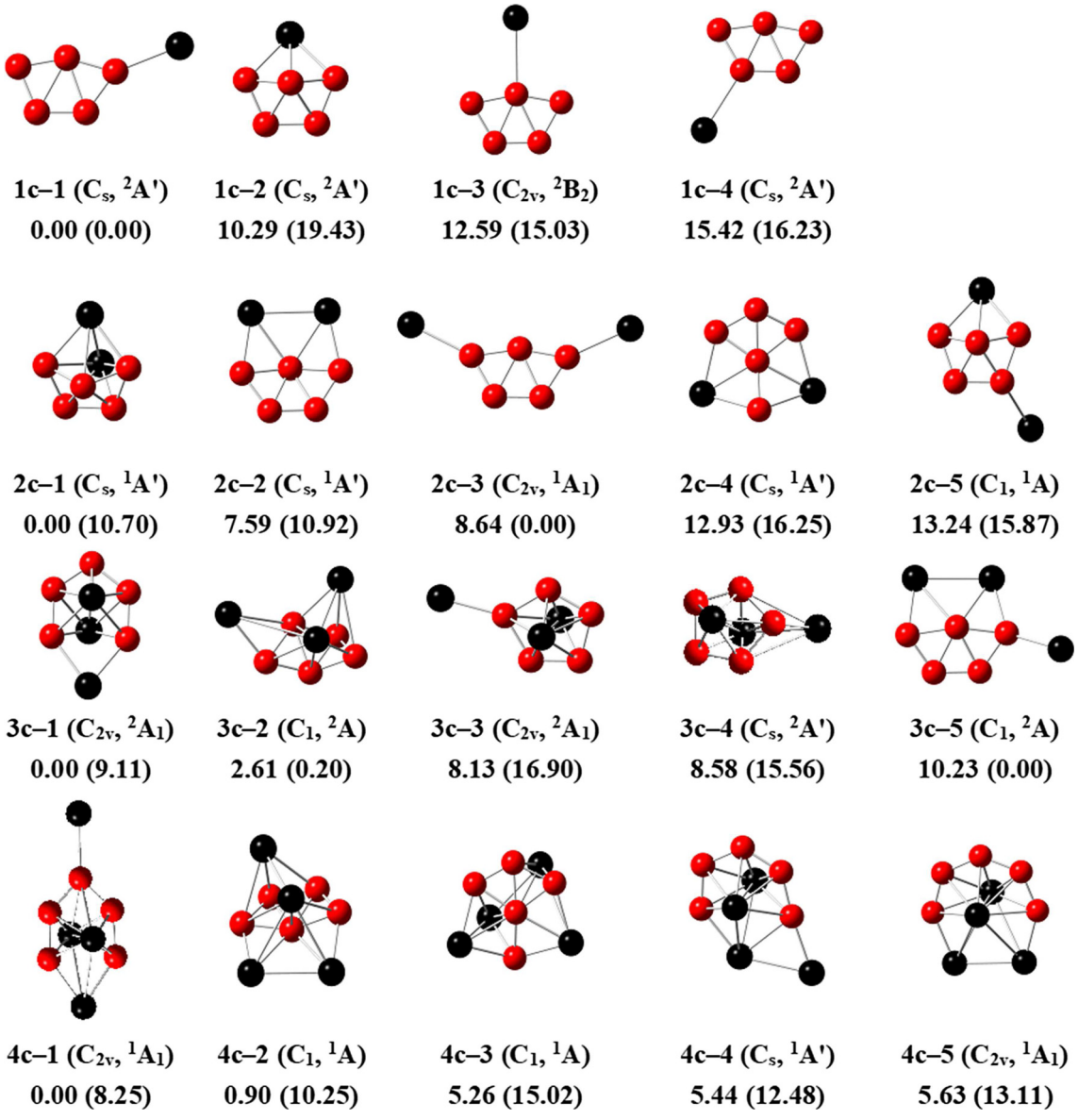


**Fig. 3.** Optimized geometries for cationic $B_5Al_n^+$ ($n=1$–4) clusters. The relative energies (in kcal/mol, under each structure) were obtained at the CCSD(T)/6–311+G(2df)//B3LYP/6–311+G(d) and B3LYP/6–311+G(d) (in parentheses) levels of theory.

$B_5Al_4^-$ isomers have higher energy than 4*a*–1 by more than 2.45 kcal/mol. Isomers 4*a*–2 and 4*a*–4 can be obtained by adding an Al atom to the periphery of structure 3*a*–1. Isomers 4*a*–3 and 4*a*–5 can be formed from structures 4*n*–3 and 4*n*–5 by electron addition.

### 3.1.3 Cationic $B_5Al_n^+$ (n = 1–4) clusters

The lower-energy isomers of cationic $B_5Al_n^+$ ($n=1$–4) clusters are shown in Figure 3, with other higher-energy isomers shown in Figure S3. For the $B_5Al^+$ cluster, the lowest energy structure 1*c*–1 with planar 2D configuration and $C_s$ symmetry is similar to structure 1*n*–2 of the neutral $B_5Al$ cluster and structure 1*a*–1 of the anionic $B_5Al^-$ cluster. The remaining three low-energy $B_5Al^+$ structures can be formed by adding an Al atom directly to the lowest energy structure of pure anionic $B_5^-$ cluster calculated by Li.[32] Since the three low-energy isomers are energetically more than 10.29 kcal/mol higher than 1*c*–1, the structure 1*c*–1 will be the global minimum of the $B_5Al^+$ cluster.

For the $B_5Al_2^+$ cluster, the lowest energy structure 2*c*–1 with 3D configuration and $C_s$ symmetry is similar to the global minimum 2*n*–1 of the neutral $B_5Al_2$ cluster. Isomer 2*c*–2 with 2D configuration and $C_s$ symmetry is similar to the neutral $B_5Al_2$ structure 2*n*–2. Isomers 2*c*–3 and 2*c*–5 can be created by adding one Al atom to the global minimum 1*c*–1 and isomer 1*c*–2 of the cationic $B_5Al^+$ cluster, respectively. Since those low-lying isomers are energetically more than 7.59 kcal/mol higher than 2*c*–1, structure 2*c*–1 will be the global minimum of the $B_5Al_2^+$ cluster.

For the $B_5Al_3^+$ cluster, the lowest energy structure 3*c*–1 with $C_{2v}$ 3D configuration and $^2A_1$ electronic state

is similar to the lowest energy structure $3n$–1 of the neutral $B_5Al_3$ cluster. Since the relative energies of the remaining isomers are higher than 2.61 kcal/mol, isomer $3c$–1 will be the global minimum of the $B_5Al_3^+$ cluster.

For the $B_5Al_4^+$ cluster, the lowest energy structure $4c$–1 with $C_{2v}$ 3D configuration and $^1A_1$ electronic state can be obtained by adding an Al atom to the global minimum $3c$–1 of the $B_5Al_3^+$ cluster. Isomer $4c$–2 has only slightly higher energy (0.90 kcal/mol) than $4c$–1. It can be created by adding two Al atoms to the surface of the $B_5Al_2^+$ structure $2c$–2. The HOMO–LUMO gap of isomer $4c$–1 is 1.82 eV, which is slightly smaller than the 2.04 eV gap of isomer $4c$–2. Therefore, both of these clusters might be observed experimentally. In addition, isomer $4c$–3 can be produced by adding two Al atoms onto the surface of the $B_5Al_2^+$ structure $2c$–4. Isomer $4c$–4 can be created by adding one Al atom to the periphery of the $B_5Al_3^+$ structure $3c$–1. Isomer $4c$–5 can be obtained by removing an electron from the global minimum $4n$–1 of the $B_5Al_4$ cluster.

### 3.2 Relative stabilities of the Al- doped boron clusters

In order to evaluate the stabilities of the neutral, anionic and cationic $B_5Al_n^{0/-/+}$ ($n$=1–4) clusters, the average binding energies $E_b$, the fragmentation energies $\Delta_1$E, and the second-order differences $\Delta_2$E were calculated, and the results are shown in Figure 4. These values were determined using the total energies of the lowest-lying $B_5Al_n^{0/-/+}$ isomers, and are defined as follows:

| | | |
|---|---|---|
| neutral | $E_b(B_5Al_n) = [5E(B) + n\,E(Al) - E(B_5Al_n)]/(5+n)$ | (1) |
| | $\Delta_1E(B_5Al_n) = E(B_5Al_{n-1}) + E(Al) - E(B_5Al_n)$ | (2) |
| | $\Delta_2E(B_5Al_n) = E(B_5Al_{n-1}) + E(B_5Al_{n+1}) - 2E(B_5Al_n)$ | (3) |
| anionic | $E_b(B_5Al_n^-) = [4E(B)+E(B^-) + nE(Al) - E(B_5Al_n^-)]/(5+n)$ | (4) |
| | $\Delta_1E(B_5Al_n^-) = E(B_5Al_{n-1}^-) + E(Al) - E(B_5Al_n^-)$ | (5) |
| | $\Delta_2E(B_5Al_n^-) = E(B_5Al_{n-1}^-) + E(B_5Al_{n+1}^-) - 2E(B_5Al_n^-)$ | (6) |
| cationic | $E_b(B_5Al_n^+) = [5E(B)+(n-1)E(Al) + E(Al^+) - E(B_5Al_n^+)]/(5+n)$ | (7) |
| | $\Delta_1E(B_5Al_n^+) = E(B_5Al_{n-1}^+) + E(Al) - E(B_5Al_n^+)$ | (8) |
| | $\Delta_2E(B_5Al_n^+) = E(B_5Al_{n-1}^+) + E(B_5Al_{n+1}^+) - 2E(B_5Al_n^+)$ | (9) |

where E(M) is the ground state energy of the entity M.

Figure 4a shows the $E_b$ values of the neutral, anionic and cationic $B_5Al_n^{0/-/+}$ ($n$=1–4) clusters. For neutral $B_5Al_n$($n$=1–4) clusters, the $E_b$ values decrease slightly, ranging from 3.53 eV to 3.38 eV. For anionic $B_5Al_n^-$ ($n$=1–4) clusters, the $E_b$ values also decrease slightly from 3.83 eV to 3.66 eV (these are typically larger than the values for the neutral clusters). For cationic $B_5Al_n^+$ ($n$=1–4) clusters, the $E_b$ values did not change significantly, ranging from 3.23 eV to 3.31 eV (these are typically smaller than the values for neutral and anionic clusters). This indicates that the anionic $B_5Al_n^-$ ($n$=1–4) clusters are slightly more stable than the neutral and cationic clusters.

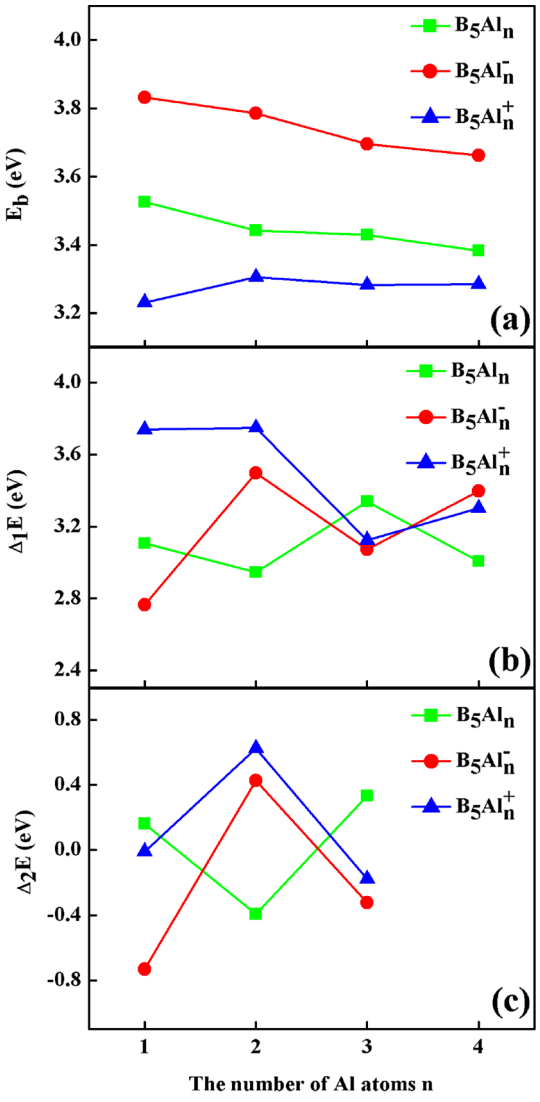


**Fig. 4.** (a) The atomic binding energies $E_b$, (b) the fragmentation energies $\Delta_1$E and (c) the second-order differences $\Delta_2$E for the lowest energy $B_5Al_n$, $B_5Al_n^-$, $B_5Al_n^+$ clusters, as a function of the number of Al atoms $n$.

Figure 4b shows the $\Delta_1E$ values of neutral, anionic and cationic $B_5Al_n^{0/-/+}$ ($n$=1–4) clusters. For neutral $B_5Al_n$($n$=1–4) clusters, the $\Delta_1E$ value with odd $n$ is greater than that with even $n$, indicating that n-odd $B_5Al_n$ clusters are more stable than n-even ones. However, for anionic $B_5Al_n^-$ ($n$=1–4) clusters, the $\Delta_1$E value with even $n$ is greater than that with odd $n$, suggesting that $n$-even $B_5Al_n^-$ clusters are more stable than $n$-odd ones. For cationic $B_5Al_n^+$ ($n$=1–4) clusters, the change in $\Delta_1$E value is significant, ranging from 3.74 eV–3.12 eV, and also the value with even n is greater than its neighbor with odd $n$.

Figure 4c shows the $\Delta_2E$ values of neutral, anionic and cationic $B_5Al_n^{0/-/+}$ ($n$=1–4) clusters. Similar to the $\Delta_1E$ results, for neutral $B_5Al_n$($n$=1–4) clusters, the $\Delta_2E$ value with odd $n$ (=1,3) is greater than that with even n (=2), indicating that $n$-odd $B_5Al_n$ clusters are more stable than

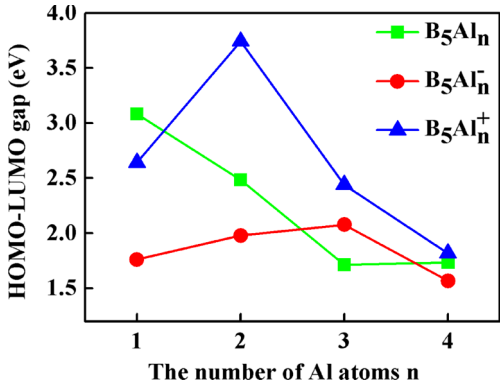


**Fig. 5.** The HOMO–LUMO gap for the lowest-energy $B_5Al_n^{0/-/+}$ structures at the B3LYP/6–311+G(d) level.

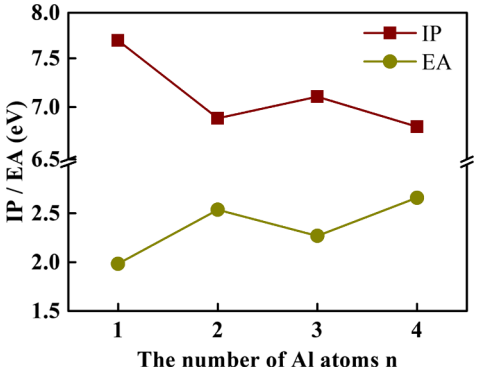


**Fig. 6.** The ionization potential (IP) and the electron affinity (EA) of the $B_5Al_n$ ($n=1$–4) clusters as a function of n.

$n$-even ones,while for ionic $B_5Al_n^{-/+}$($n=1$–4) clusters, the $\Delta_2E$ value with even n is greater than that with odd $n$, suggesting that $n$-even $B_5Al_n^{-/+}$ clusters are more stable than $n$-odd ones.

The HOMO–LUMO gap, the energy difference between HOMO and LUMO, can illuminate the stability of the clusters. The wider the gap, the more stable the cluster. The HOMO–LUMO gaps for the lowest energy structures of the $B_5Al_n^{0/-/+}$ ($n=1$–4) clusters are shown in Figure 5. For neutral $B_5Al_n$ ($n=1$–4) clusters, as n is increase, the HOMO–LUMO gaps are significantly reduced from 3.08 eV to 1.71 eV. For anionic $B_5Al_n^-$ ($n=1$–4) clusters, the gaps first rise and then fall over a range of 1.57 eV to 2.08 eV. For cationic $B_5Al_n^+$ ($n=1$–4) clusters, the gaps first rise and then fall (between 1.82 eV and 3.74 eV). The maximum in this case occurs at $n=2$, indicating that the chemical stability of the $B_5Al_2^+$ cluster is higher than the other clusters, which is consistent with the earlier result from Figure 4c.

The ionization potential (IP) and electron affinity (EA) measure the ability of a cluster to lose and gain electrons. Clusters with larger IP values require more energy to remove an electron, and therefore are more likely to be stable. Clusters with large EA values can aquire an extra electron more easily, and therefore the anionic cluster will be more stable. The IP and EA values for $B_5Al_n$ ($n=1$–4) clusters can be calculated using equations 10 and 11:

| | |
|---|---|
| $IP(B_5Al_n) = E$(optimized cation $B_5Al_n^+$) − $E$(optimized neutral $B_5Al_n$) | (10) |
| $EA(B_5Al_n) = E$(optimized neutral $B_5Al_n$) − $E$(optimized anion $B_5Al_n^-$) | (11) |

As shown in Figure 6, the IP values range from 7.69 eV to 6.81 eV. The $n$-odd clusters have larger IP than their $n$-even neighbors, indicating that the $n$-odd clusters hold onto electrons more strongly than the $n$-even ones. This is consistent with the results from Figures 4b and 4c. The EA values range from 1.98 eV to 2.54 eV. The $n$-even clusters have larger EA than their $n$-odd neighbors, suggesting that the $n$-even clusters are more likely to obtain electrons than the $n$-odd clusters.

### 3.3 Simulated spectra

To provide further insight into the understanding of future infrared and photo-electron spectroscopy experimental measurements, computational frequency analysis and VDE simulation were performed for each cluster. These results are shown in Figures 7 and 8, respectively. IR spectra can facilitate the determination of the $B_5Al_n^{0/-/+}$ structures in future experimental measurements, while PE spectra can generally be used as a fingerprint for anionic clusters.

#### 3.3.1 Calculated infrared spectra

As shown in Figure 7, structure 1$n$–1 has the strongest absorption peak at 679 $cm^{-1}$, which originates from the stretching vibration of the five boron atoms. For structure 1$a$–1, the main peak is located at 1165 $cm^{-1}$. Other weaker absorption bands are at lower frequencies, and are much lower in intensity. For structure 1$c$–1, the two main peaks at 1076 $cm^{-1}$ and 1230 $cm^{-1}$ correspond to vibrations of the five boron atoms. For the $B_5Al_2^{0/-/+}$ clusters, the IR spectral shapes are much more complicated. For structure 2$n$–1, there are three main peaks, which are located at 386 $cm^{-1}$, 766 $cm^{-1}$ and 1034 $cm^{-1}$ respectively. For structure 2$a$–1, there are two main peaks located at 354 $cm^{-1}$ and 738 $cm^{-1}$, respectively (these mainly originate from various vibrations of the five boron atoms). For structure 2$c$–1, there is a stronger absorption peak at 1172 $cm^{-1}$, and other weaker absorption peaks are at lower frequencies. For structure 3$n$–1, there are two main peaks at 471 $cm^{-1}$ and 897 $cm^{-1}$, respectively (these mainly derive from various vibrations of the five boron atoms). For structure 3$a$–1, there is a stronger absorption peak at 491 $cm^{-1}$, while many other weaker absorption peaks also are seen. For structure 3$c$–1, the strongest absorption peak is at 369 $cm^{-1}$, which mainly originates from the stretching vibration of the six-membered ring. For 4$n$–1, there are stronger absorption peaks at 417 $cm^{-1}$ and 1340 $cm^{-1}$, which are different vibration modes mainly from the five boron atoms. Structure 4$a$–1 and 4$c$–1 have the strongest absorption peak at 1245 $cm^{-1}$ and 920 $cm^{-1}$, respectively, which both correspond to the stretching vibration of five boron atoms.

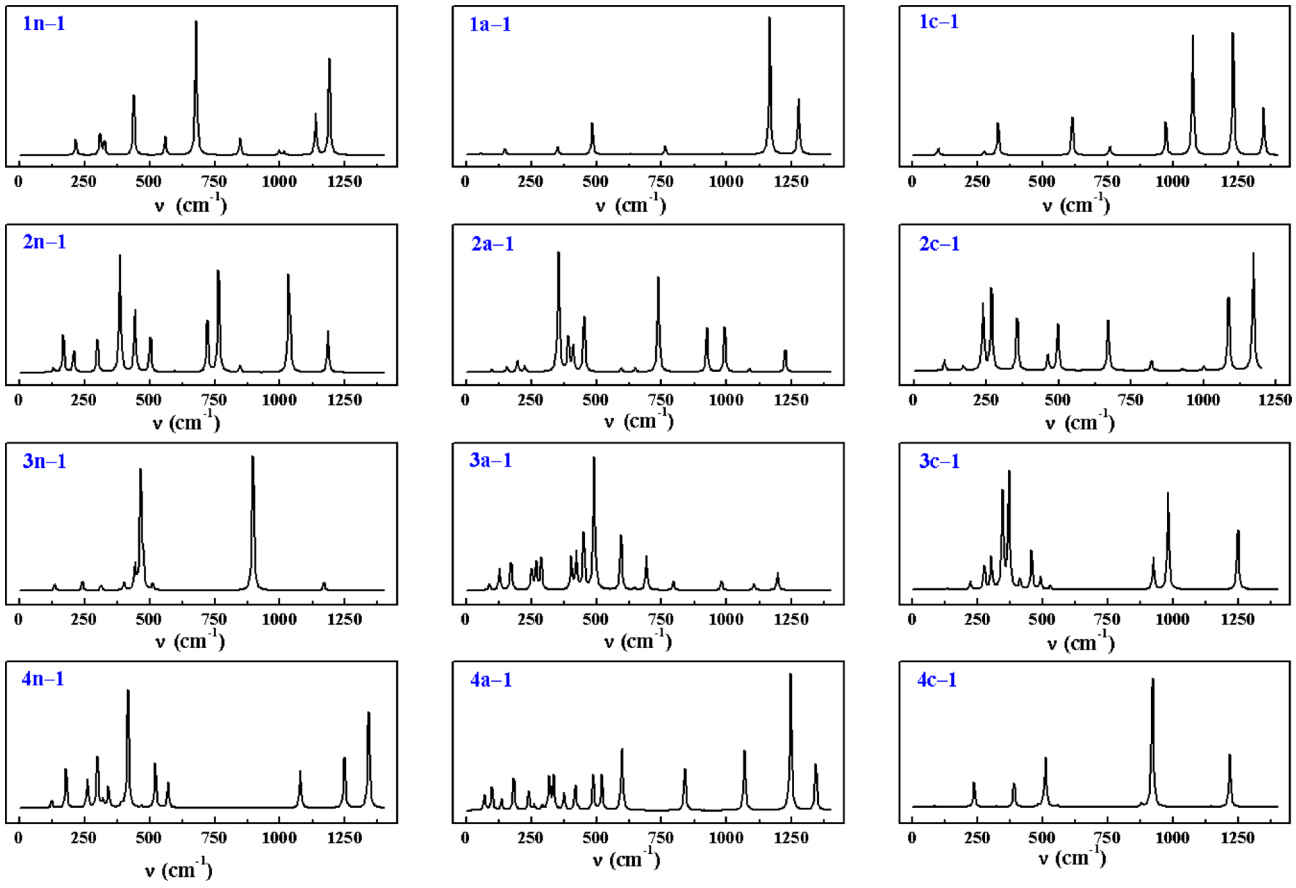


**Fig. 7.** Calculated IR spectra for the lowest-energy structures of the $B_5Al_n^{0/-/+}$ ($n=1$–4) clusters at the B3LYP/6–311+G(d) level.

### 3.3.2 Simulated photoelectron spectra

The simulated PE spectra for anionic $B_5Al_n^-$ clusters are shown in Figure 8, with the calculated VDEs, using the TD-DFT method at the TD-B3LYP/6–311+G(d) level. The corresponding final electronic configurations are listed in Tables S1–S4.

As shown in Figure 8, the first VDE peak of structure 1*a*–1 is at 2.22 eV. This is a result of detaching one electron from a singly occupied molecular orbital (SOMO). The second VDE corresponds to detaching one electron from its HOMO-1, producing the first triplet state at 2.66 eV. The remaining singlet and triplet peaks are observed in the range of 2.99 eV–4.52 eV. The simulated spectra for 2*a*–1 reveal that the first VDE at 2.75 eV comes from electron detachment from its HOMO. The second and third VDEs are obtained by detaching one electron from its HOMO-1 and HOMO-2 at 3.43 and 3.76 eV. The fourth VDE at 3.94 eV overlaps the fifth VDE at 3.99 eV, forming the fourth peak and corresponding to an electron detachment from the HOMO-3. The remaining peaks for 2*a*–1 are in the range of 4.20 eV–4.74 eV. Similar to 1*a*–1, for 3*a*–1, the simulated PE spectra shows that there are many strong peaks which are very close to each other. The first VDE peak at 2.85 eV rises from electron detachment from its SOMO. The second VDE is at 3.05 eV, and is obtained by detaching one electron from its HOMO-1 resulting in the first triplet state. The third peak is formed by the overlap of the third VDE at 3.48 eV and the fourth VDE at 3.54 eV. There are many VDEs in the range of 3.80 eV–4.31 eV. For 4*a*–1, the first VDE at 2.65 eV comes from detaching one electron from its HOMO (similar to 2*a*–1). The second VDE at 3.34 eV corresponds to electron detachment from its HOMO-1, and other intense peaks range from 3.45 eV to 4.48 eV.

## 3.4 Chemical bonding analysis

Chemical bonding is very important in chemistry. From the chemical bonding analysis, we can understand the relationship between the component atoms and the stability of the cluster. In this paper, the chemical bonds for the most stable structures of each $B_5Al_n^{0/-/+}$ cluster were analyzed by the AdNDP method. AdNDP is based on the concept of the electron pair as the main element of chemical bonding models. AdNDP represents the electronic structure in terms of nc–2e bonds, where n is the number of atoms included in a multi-center bond. This allows the identification of multi-center bonds in addition to normal two-center classical bonds. The AdNDP bonding patterns for the most stable $B_5Al_n^{0/-/+}$ structures are displayed in Figures 9–12. The occupation numbers (ON) for each

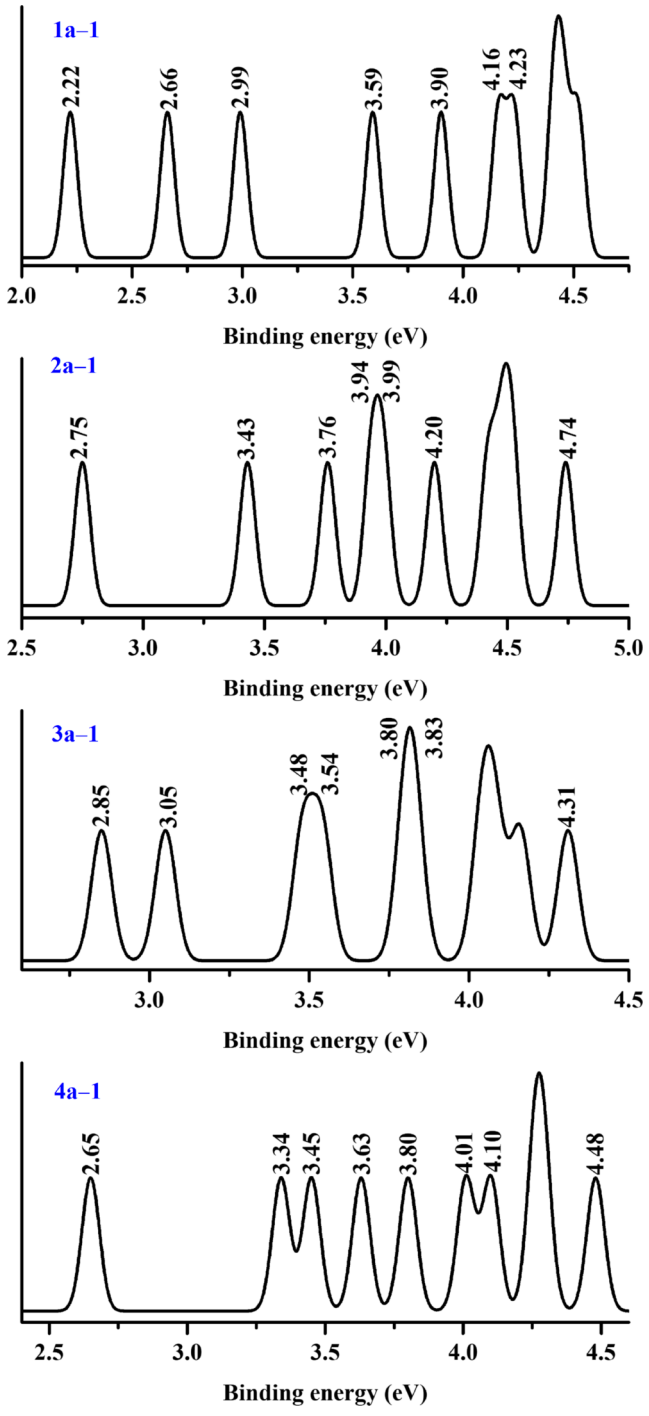


**Fig. 8.** Simulated PE spectra for the lowest-energy $B_5Al_n^-$ ($n = 1$–4) structures obtained using the TD-B3LYP/6–311+G(d) method with vertical detachment energies (VDE) indicated.

individual chemical bond are shown. The ideal ON value for a saturated bond is 2.0 |e|, but there are some variations from this observed. On the other hand, we can also evaluate the strength of the interaction between two atoms by the bond distance. In this paper, we use the sum of single bond radii of boron and boron ($R_{B-B} = r_B + r_B = 1.70$ Å), of boron and aluminum ($R_{B-Al} = r_B + r_{Al} = 2.11$ Å) and of aluminum and aluminum ($R_{Al-Al} = r_{Al} + r_{Al} = 2.52$ Å) [35] as reference bond distances. We can then compare the calculated bonding of the clusters to the reference bond distances.

### 3.4.1 Chemical bonding of the $B_5Al^{0/-/+}$ clusters:

As shown in Figure 9, the AdNDP bond analysis of the $B_5Al^{0/-/+}$ clusters shows that they have delocalized $\sigma$ and $\pi$ bonds. For the neutral $B_5Al$ structure 1$n$–1, there are two B–Al $\sigma$ bonds, five peripheral 2$c$–2e B–B $\sigma$ bonds in the W-like $B_5$ core, a delocalized 5$c$–2e $\sigma$ bond, and a delocalized 5$c$–2e $\pi$ bond over the molecular plane. Similarly, for the anionic $B_5Al^-$ structure 1$a$–1, there is one peripheral B–Al $\sigma$ bond, five peripheral 2$c$–2e B–B $\sigma$ bonds in the W–like $B_5$ core, one delocalized 5$c$–2e $\sigma$ bond, and one delocalized 5$c$–2e $\pi$ bond over the molecular plane. Furthermore, structure 1$a$–1 possesses a lone pair (LP) on the Al atom (ON = 1.95 |e|) which is presumably due to the neutral $B_5Al$ cluster having gained one electron. The cationic $B_5Al^+$ cluster also has a B–Al $\sigma$ bond, five peripheral 2$c$–2e B–B $\sigma$ bonds in the $B_5$ core, a delocalized 5$c$–2e $\sigma$ bond, and a delocalized 5$c$–2e $\pi$ bond. Structure 1$c$–1 has no LP on the Al atom, which may be because the neutral $B_5Al$ cluster has lost an electron.

The five peripheral B=B bond lengths in structure 1$n$–1 range from 1.579 Å to 1.586 Å. These are slightly longer than the sum of the double bond radii of boron (1.56 Å) but much shorter than the sum of the single bond radii of boron (1.70 Å). This indicates that the B=B has double bond character, which is consistent with the five peripheral 2$c$–2e B–B $\sigma$ bonds and the two 5$c$–2e delocalized bonds in the $B_5$ unit predicted by the AdNDP analysis above. The two internal B–B bond lengths in structure 1$n$–1 are 1.742 Å, which is somewhat longer than that of the B–B single bond (1.70 Å), corresponding to slightly weakened B–B single bonds. Therefore there are no direct 2$c$–2e B–B bonds between them other than the two 5$c$–2e delocalized bonds in the $B_5$ unit, as shown by the AdNDP analysis. The B–Al bond lengths in structure 1$n$–1 are 2.231 Å, which is close to the sum of the single bond radii of boron and aluminum (2.11 Å), and 2$c$–2e B–Al $\sigma$ bonds are also present in the AdNDP results. Similarly, the bond lengths in structures 1$a$–1 and 1$c$–1 also correspond to their AdNDP results. The five peripheral B=B bond lengths in structures 1$a$–1 and 1$c$–1 are 1.521 Å to 1.663 Å and 1.549 Å to 1.591 Å, respectively, which are similar to the sum of the double bond radii of boron (1.56 Å), indicating they are B=B double bonds. The two internal B–B bond lengths in structures 1$a$–1 and 1$c$–1 are 1.734 Å to 1.802 Å and 1.819 Å to 1.952 Å, respectively. These are slightly longer than the standard B–B single bond of 1.70 Å, suggesting that they are weaker B–B single bonds. The B–Al bond lengths in structures 1$a$–1 and 1$c$–1 are 2.079 Å and 2.183 Å, respectively. These lengths are close to the sum of the single bond radii of boron and aluminum (2.11 Å), indicating that they are B–Al single bonds. Therefore, in structures 1$n$–1, 1$a$–1, and 1$c$–1, the $B_5$ ring has five B = B double bonds on the

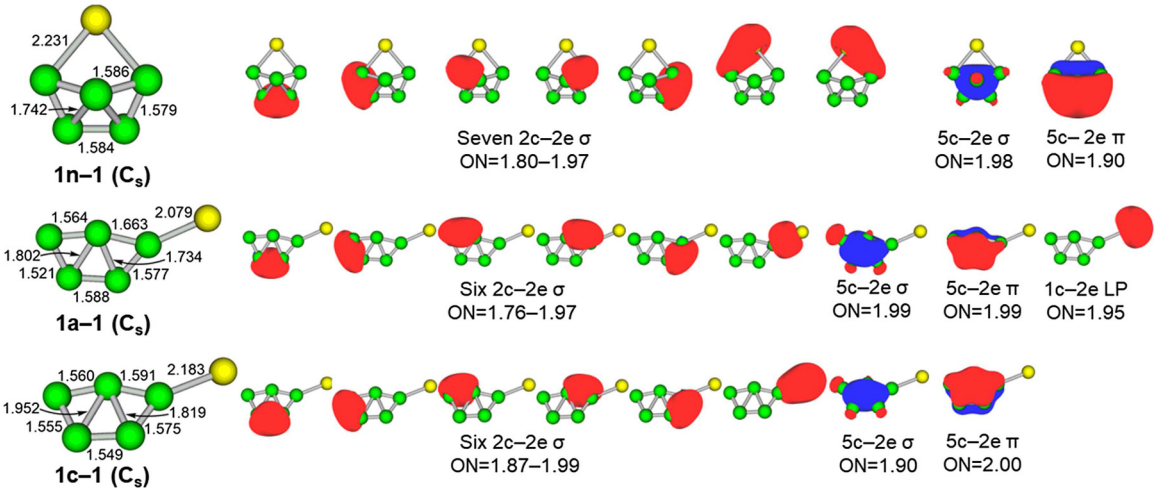


**Fig. 9.** AdNDP bonding pattern for the lowest energy structures of the $B_5Al$, $B_5Al^-$ and $B_5Al^+$clusters.

periphery. The presence of two $5c$–2e delocalized bonds makes the $B_5$ ring have a strong conjugate effect and adds additional stability, which may be the reason why the Al atoms are preferentially located on the periphery of the ring.

### 3.4.2 Chemical bonding of the $B_5Al_2^{0/-/+}$ clusters:

Figure 10 shows that the neutral $B_5Al_2$ structure $2n$–1, and the cationic $B_5Al_2^+$ have very similar AdNDP bonding patterns: a LP on the Al atom, five $2c$–2e B–B/B–Al $\sigma$ bonds, three $3c$–2e bonds, and one $5c$–2e delocalized $\sigma$ bond. For the anionic $B_5Al_2^-$ structure $2a$–1, there are two LPs on the two Al atoms, five $2c$–2e B–B/B–Al $\sigma$ bonds, three $3c$–2e delocalized $\sigma$ bonds, and one $5c$–2e delocalized $\pi$ bond. The bond lengths in structures $2n$–1, $2a$–1, and $2c$–1 are also consistent with the bonding pattern predicted by the AdNDP analysis above. The B=B bond lengths of 1.558 Å to 1.607 Å (in $2n$–1), 1.565 Å to 1.603 Å (in $2a$–1), and 1.584 Å to 1.592 Å (in $2c$–1) are similar to the sum of the double bond radii of boron (1.56 Å), corresponding to B = B double bonds. The other B–B bond lengths of 1.674 Å to 1.696 Å (in $2n$–1), 1.669 Å to 1.717 Å (in $2a$–1), and 1.622 Å to 1.732 Å (in $2c$–1) are close to the sum of the single bond radii of boron (1.70 Å), suggesting B–B single bonds. The B–Al bond lengths of 2.116 Å (in $2n$–1), 2.097 – 2.151 Å (in $2a$–1), and 2.136 Å (in $2c$–1), are close to the sum of the radii of single bonds of boron and aluminum (2.11 Å), indicating B–Al single bonds. The other B–Al bonds with longer distances correspond to very weak B–Al bonds. The Al–Al bond lengths of 3.011 Å, 2.810 Å, and 2.798 Å, in $2n$–1, $2a$–1, and $2c$–1, respectively, are longer than the sum of the single bond radii of aluminum (2.52 Å), indicating very weak Al–Al bonds, so they do not appear in the AdNDP results.

### 3.4.3 Chemical bonding of the $B_5Al_3^{0/-/+}$ clusters:

As shown in Figure 11, the neutral $B_5Al_3$ structure $3n$–1, and the cationic $B_5Al_3^+$ structure $3c$–1 also have similar AdNDP bonding: seven $2c$–2e B–B/B–Al $\sigma$ bonds, one $6c$–2e $\pi$ bond, two $7c$–2e $\sigma/\pi$ bonds, and one $8c$–2e delocalized $\pi$ bond. Furthermore, structure $3n$–1 has one more $3c$–2e delocalized $\sigma$ bond. For the anionic $B_5Al_3^-$ structure $3a$–1, there is one LP on an Al atom, six $2c$–2e B-B/B-Al $\sigma$ bonds, two $4c$–2e delocalized $\sigma$ bonds, two $5c$–2e delocalized $\sigma$ bonds, and one $6c$–2e delocalized $\pi$ bond. Combined with the AdNDP analyses above, the B=B bonds with lengths 1.557 Å to 1.625 Å (in $3n$–1), 1.555 Å to 1.579 Å (in $3a$–1), and 1.549 Å to 1.592 Å (in $3c$–1), are similar to the sum of the double bond radii of boron (1.56 Å), and will be B=B double bonds. The B–B bonds with lengths 1.702 Å to 1.735 Å in $3a$–1, are close to the sum of the single bond radii of boron (1.70 Å), and should be considered B–B single bonds. The B–Al bonds with lengths 2.098 Å to 2.490 Å (in $3n$–1), 2.061 Å to 2.335 Å (in $3a$–1), and 2.066 Å to 2.442 Å (in $3c$–1), are similar to the sum of the single bond radii of boron and aluminum (2.11 Å), and are therefore B–Al single bonds. The Al–Al bond length in structure $3a$–1 is 2.650 Å which is close to the sum of the single bond radii of aluminum (2.52 Å), and the AdNDP analysis shows that this is a $2c$–2e Al–Al $\sigma$ bond.

### 3.4.4 Chemical bonding of the $B_5Al_4^{0/-/+}$ clusters:

Figure 12 shows the neutral $B_5Al_4$ structure $4n$–1 has seven $2c$–2e B–B/B–Al $\sigma$ bonds, one $5c$–2e $\pi$ bond, two $6c$–2e $\sigma$ bonds, two $6c$–2e $\pi$ bonds, and one $9c$–2e delocalized $\sigma$ bond. For the anionic $B_5Al_4^-$ structure $4a$–1, there are eight $2c$–2e B–B/B–Al $\sigma$ bonds, two $5c$–2e $\pi$ bonds, two $6c$–2e $\sigma$ bonds, one $8c$–2e $\sigma$ bond, and one $8c$–2e delocalized $\pi$ bond. The cationic $B_5Al_4^+$ structure $4c$–1 has similar bonding to the $B_5Al_3^+$ structure $3c$–1: eight $2c$–2e B–B/B–Al $\sigma$ bonds, one $4c$–2e $\sigma$ bond, one $6c$–2e $\pi$ bond, one $7c$–2e $\sigma$ bond, one $7c$–2e $\pi$ bond, and one $8c$–2e delocalized $\pi$ bond. Based on the AdNDP analysis above, the B=B bonds with lengths 1.553 Å to 1.555 Å (in $4n$–1), 1.549 Å to 1.563 Å (in $4a$–1), and 1.584 Å to 1.600 Å (in $4c$–1) should be B=B double bonds. This is consistent

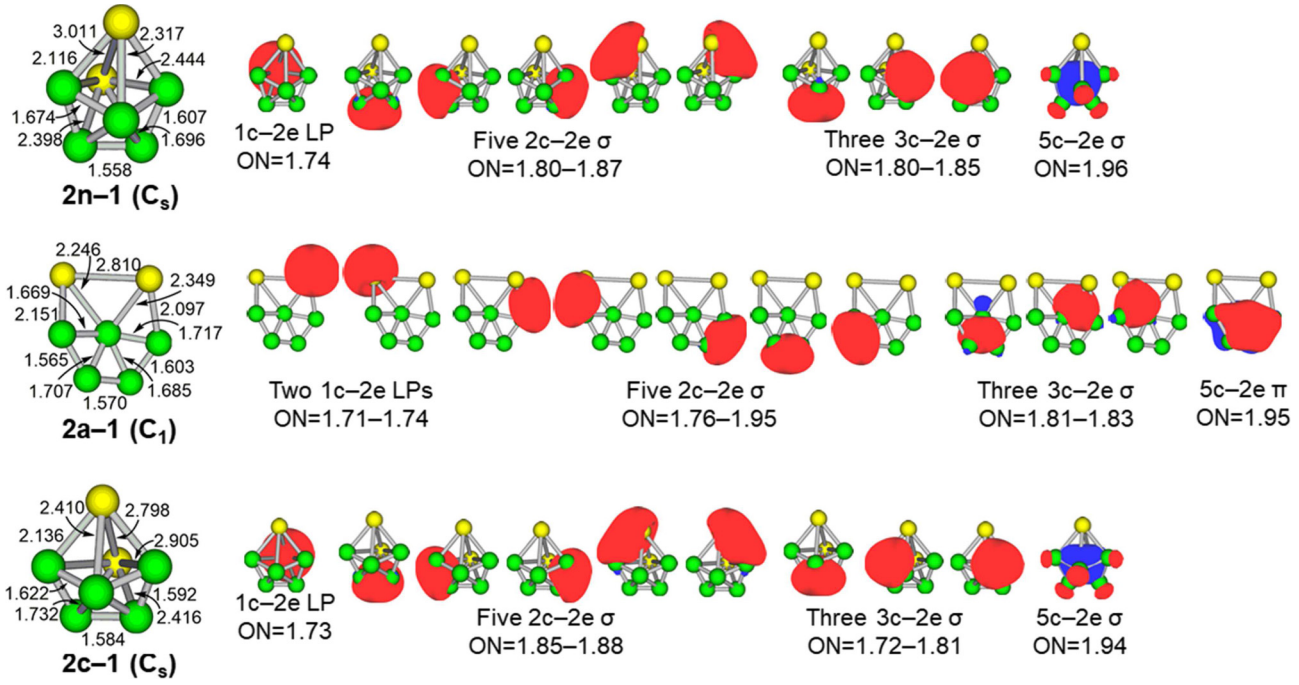


**Fig. 10.** AdNDP bonding pattern for the lowest energy structures of the $B_5Al_2$, $B_5Al_2^-$ and $B_5Al_2^+$ clusters.

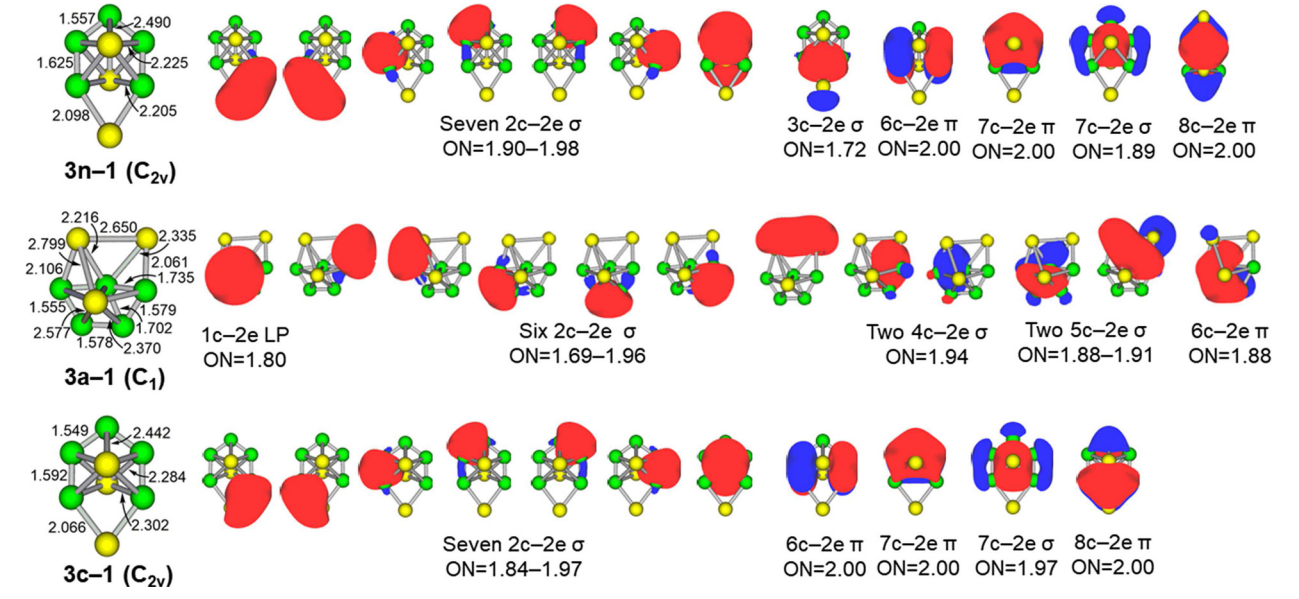


**Fig. 11.** AdNDP bonding pattern for the lowest energy structures of the $B_5Al_3$, $B_5Al_3^-$ and $B_5Al_3^+$ clusters.

with the bond length 1.56 Å of the B=B double bond from the sum of the double bond radii of boron. The B–Al bonds with lengths 2.009 Å to 2.321 Å (in 4*n*–1), 2.001 Å to 2.400 Å (in 4*a*–1), and 2.055 Å to 2.253 Å (in 4*c*–1) should be B–Al single bonds. This is consistent with the bond length 2.11 Å of the B–Al single bond from the sum of the single bond radii of boron and aluminum. Structure 4*c*–1 has a B–Al bond length of 2.659 Å, which corresponds to a weaker B–Al single bond. The Al–Al bond lengths in structures 4*n*–1 and 4*a*–1 are 2.497 Å to 2.792 Å and 2.526 Å to 2.707 Å, respectively. These are close to the sum of the single bond radii of aluminum and aluminum (2.52 Å), so they should be Al–Al single bonds. Structure 4*c*–1 has a longer Al–Al bond length of 2.966 Å, which corresponds to a weaker Al–Al single bond.

In summary, for the $B_5Al_n^{0/-/+}$ ($n=1$–4) systems, the bond orders based on the bond lengths are consistent with the AdNDP results. Our AdNDP analyses show some multicenter delocalized bonding in the $B_5Al_n^{0/-/+}$ systems. The delocalized bonds in the $B_5Al^{0/-/+}$ and $B_5Al_2^{0/-/+}$ systems cross the W-like $B_5$ ring, which enhances the

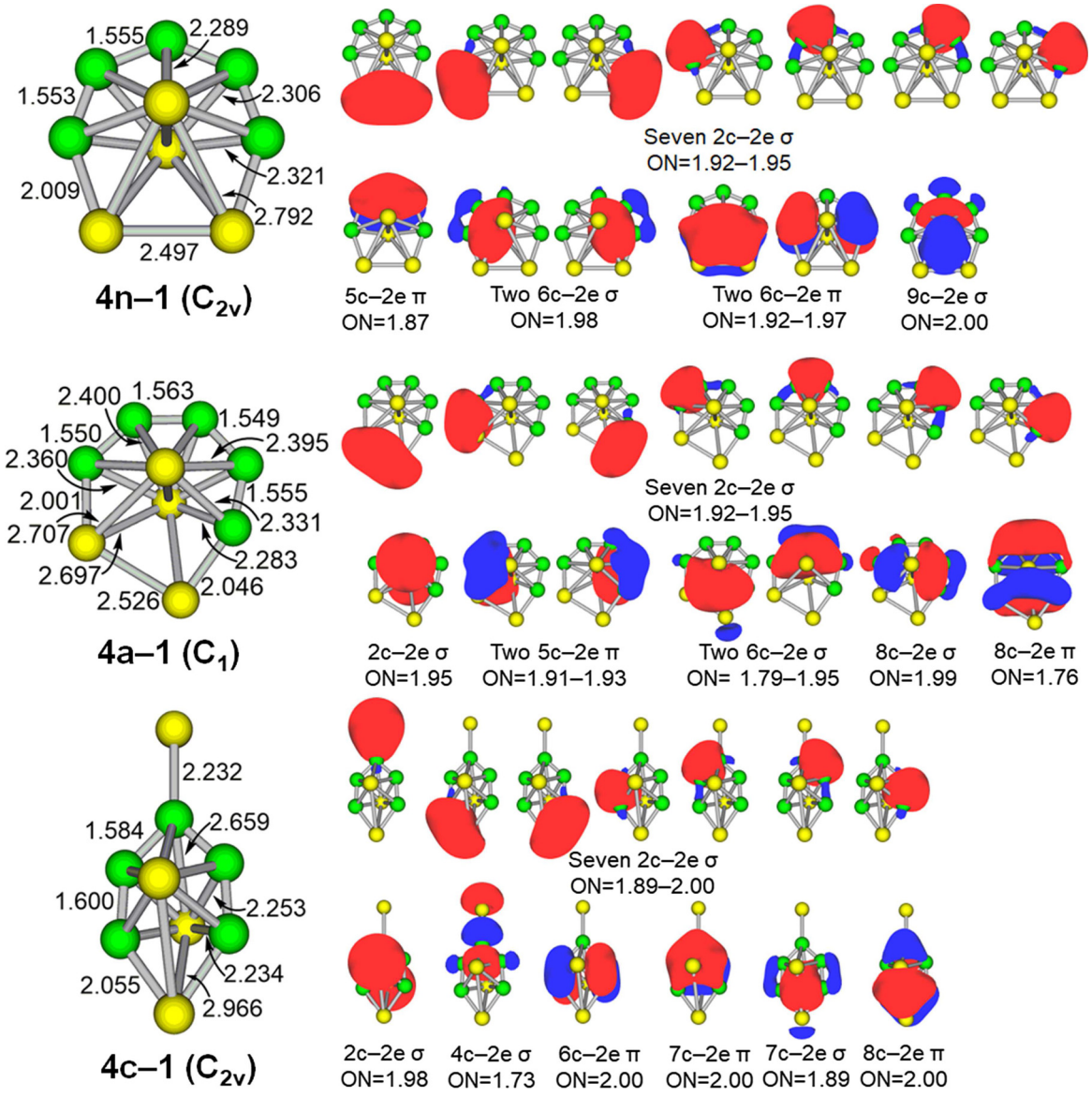


**Fig. 12.** AdNDP bonding pattern for the lowest energy structures of the $B_5Al_4$, $B_5Al_4^-$ and $B_5Al_4^+$ clusters.

stability of the $B_5$ unit and causes the Al atom(s) to be preferentially located outside the $B_5$ ring. For the $B_5Al_3^{0/+}$ and $B_5Al_4^{0/-/+}$ systems, there is enough energy to open the $B_5$ unit and place Al atom(s) amongst the B atoms, maybe since their 6 $\pi$ electrons satisfy the 4n + 2 rule for aromaticity ($n=1$) and enhance the stability of the cluster. The $B_5Al_3^-$ cluster can be seen as a turning point. Although there is also a W-like $B_5$ ring, the delocalized bonds on the $B_5$ ring are dispersed, due to the action of three Al atoms, and the 6$\pi$ aromaticity also exists, which results in some stability.

## 4 Summary

In this paper, binary boron-aluminum $B_5Al_n^{0/-/+}$ ($n=1$–4) clusters were systematically studied using DFT and CCSD(T) methods, at the B3LYP/6–311+G(d) and CCSD(T)/6–311+G(2df) levels, to understand their geometric structures, stabilities, electronic properties, and chemical bonding. For one or two Al atoms, the lowest energy $B_5Al_n^{0/-/+}$ structures have the five boron atoms preferentially forming a W-like structure with the Al atoms at the periphery. For three or four Al atoms, the clusters have their lowest energy structures in a bipyramidal configuration. The binding energy results show that the anionic $B_5Al_n^-$ ($n=1$–4) clusters are more stable than their corresponding neutral and cationic clusters. The $\Delta_1E$ and $\Delta_2E$ results show that neutral $B_5Al_n$($n=1$, 3) clusters are more stable than neutral $B_5Al_n$($n=2$,4) clusters, while anionic and cationic $B_5Al_n$($n=2$, 4) are more stable than neutral $B_5Al_n$($n=1$, 3). The HOMO–LUMO gaps illustrate that the $B_5Al_2^+$ cluster has the highest chemical stability among the $B_5Al_n^{0/-/+}$ ($n=1$–4)

clusters. The IP values for the neutral $B_5Al_n$ clusters are consistent with the $\Delta_1$E and $\Delta_2 E$ results. The EA values show that neutral $B_5Al_n(n=2, 4)$ clusters can more easily obtain electrons than n-odd $B_5Al_n$ clusters. AdNDP analysis shows that there are a variety of delocalized multicenter bonds in the clusters. This explains why the Al atoms are preferentially located at the periphery of the $B_5$ ring. The existence of the 4n + 2 rule 6 $\pi$ delocalized bonds indicates that some of the clusters have aromaticity, which may enhance their stablities.

L. M. W and L.-M. Y. gratefully acknowledge support from the National Natural Science Foundation of China (21673087, 21873032, 21903032, 22073033), startup fund (2006013118 and 3004013105) from Huazhong University of Science and Technology, and the Fundamental Research Funds for the Central Universities (2019kfyRCPY116). The authors thank the Minnesota Supercomputer Institute for computational resources.

## Author contribution statement

Limei Wen: performed computations, collected and analyzed the data, and wrote the draft of the paper. Guoliang Li: provided computational resources, designed and performed research, analyzed data, and revised the draft of the paper. Li-Ming Yang: conceived the study, designed and performed research, analyzed data, and revised both draft and final paper. Eric Ganz: provided computational resources, revised the paper, and reviewed the final paper.



## References

1. B. Qi, C. Wu, X. Li, D. Wang, L. Sun, B. Chen, W. Liu, H. Zhang, X. Zhou, ChemCatChem **10**, 2285 (2018)
2. D. Tu, S. Cai, C. Fernandez, H. Ma, X. Wang, H. Wang, C. Ma, H. Yan, C. Lu, Z. An, Angew. Chem. Int. Ed. **58**, 9129 (2019)
3. W.L. Li, X. Chen, T. Jian, T.T. Chen, J. Li, L.S. Wang, Nat. Rev. Chem. **1**, 0071 (2017)
4. L.S. Wang, Int. Rev. Phys. Chem. **35**, 69 (2016)
5. H.-J. Zhai, B. Kiran, J. Li, L.S. Wang, Nat. Mater. **2**, 827 (2003)
6. A.N. Alexandrova, A.I. Boldyrev, H.-J. Zhai, L.S. Wang, Coord. Chem. Rev. **250**, 2811 (2006)
7. J. Warneke, G.-L. Hou, E. Aprà, C. Jenne, Z. Yang, Z. Qin, K. Kowalski, X.-B. Wang, S.S. Xantheas, J. Am. Chem. Soc. **139**, 14749 (2017)
8. J. Warneke, S.Z. Konieczka, G.-L. Hou, E. Aprà, C. Kerpen, F. Keppner, T.C. Schäfer, M. Deckert, Z. Yang, E.J. Bylaska, G.E. Johnson, J. Laskin, S.S. Xantheas, X.-B. Wang, M. Finze, Phys. Chem. Chem. Phys. **21**, 5903 (2019)
9. M. Mayer, V. van Lessen, M. Rohdenburg, G.L. Hou, Z. Yang, R.M. Exner, E. Apra, V.A. Azov, S. Grabowsky, S.S. Xantheas, K.R. Asmis, X.B. Wang, C. Jenne, J. Warneke, Proc. Natl. Acad. Sci. USA **116**, 8167 (2019)
10. M. Rohdenburg, Z. Yang, P. Su, E. Bernhardt, Q. Yuan, E. Apra, S. Grabowsky, J. Laskin, C. Jenne, X.-B. Wang, J. Warneke, Phys. Chem. Chem. Phys. **22**, 17713 (2020)
11. E. Apra, J. Warneke, S.S. Xantheas, X.B. Wang, J. Chem. Phys. **150**, 164306 (2019)
12. N.M. Tam, L.V. Duong, H.T. Pham, M.T. Nguyen, M.P. Pham-Ho, Phys. Chem. Chem. Phys. **21**, 8365 (2019)
13. A. Kumar, N. Vyas, A. K. Ojha, Int. J. Hydrogen Energy **45**, 12961 (2020)
14. D. Kang, W. Sun, H. Shi, C. Lu, X. Kuang, B. Chen, X. Xia, G. Maroulis, Sci. Rep. **9**, 14367 (2019)
15. C. Romanescu, A.P. Sergeeva, W.-L. Li, A.I. Boldyrev, L.-S. Wang, J. Am. Chem. Soc. **133**, 8646 (2011)
16. W.-L. Li, C. Romanescu, T.R. Galeev, L.-S. Wang, A.I. Boldyrev, J. Phys. Chem. A **115**, 10391 (2011)
17. T.R. Galeev, C. Romanescu, W.-L. Li, L.-S. Wang, A.I. Boldyrev, J. Chem. Phys. **135**, 104301 (2011)
18. B. Song, Y. Zhou, H.-M. Yang, J.-H. Liao, L.-M. Yang, X.-B. Yang, E. Ganz, J. Am. Chem. Soc. **141**, 3630 (2019)
19. L. Wen, G. Li, L.-M. Yang, H. Pan, E. Ganz, Mater. Today Commun. **24**, 100914 (2020)
20. A.P. Sergeeva, B.B. Averkiev, H.J. Zhai, A.I. Boldyrev, L.-S. Wang, J. Chem. Phys. **134**, 224304 (2011)
21. A.D. Becke, J. Chem. Phys. **98**, 5648 (1993)
22. C. Lee, W.T. Yang, R.G. Parr, Phys. Rev. B **37**, 785 (1988)
23. J.S. Binkley, J.A. Pople, W.J. Hehre, J. Am. Chem. Soc. **102**, 939 (1980)
24. M.S. Gordon, J.S. Binkley, J.A. Pople, W.J. Pietro, W.J. Hehre, J. Am. Chem. Soc. **104**, 2797 (1982)
25. G.D. Purvis, R.J. Bartlett, J. Chem. Phys. **76**, 1910 (1982)
26. D.Y. Zubarev, A.I. Boldyrev, Phys. Chem. Chem. Phys. **10**, 5207 (2008)
27. D.Y. Zubarev, A.I. Boldyrev, J. Org. Chem. **73**, 9251 (2008)
28. D.Y. Zubarev, A.I. Boldyrev, J. Phys. Chem. A **113**, 866 (2009)
29. D.Y. Zubarev, N. Robertson, D. Domin, J. McClean, J. Wang, W. A. Lester Jr, R. Whitesides, X. You, M.J. Frenklach, Phys. Chem. C **114**, 5429 (2010)
30. M. Frisch, G. Trucks, H. Schlegel, G. Scuseria, M. Robb, J. Cheeseman, G. Scalmani, V. Barone, B. Mennucci, G. Petersson, *Gaussian 09, Revision A. 02.* (Gaussian Inc., Wallingford, CT., 2009)
31. T. Lu, F. Chen, J. Comput. Chem. **33**, 580 (2012)
32. Q.S. Li, H.W. Jin, J. Phys. Chem. A **106**, 7042 (2002)
33. X.-J. Feng, Y.-H. Luo, J. Phys. Chem. A **111**, 2420 (2007)
34. M. Böyükata, Z.B. Güvenç, J. Alloys Compd. **509**, 42144234 (2011)
35. P. Pyykkö, J. Phys. Chem. A **119**, 2326 (2015)